Arrays of Annular Antennas With SINIS Bolometers

Mikhail A. Tarasov, Aleksandra A. Gunbina, Sumedh Mahashabde, Renat A. Yusupov, Artem M. Chekushkin, Daria V. Nagirnaya, Valerian S. Edelman, Grigory V. Yakopov, and Vyacheslav F. Vdovin

***Abstract*—For improving the dynamic range and sensitivity at high power load, we have integrated superconductor-insulator-normal metal-insulator-superconductor (SINIS) bolometers with a frequency selective surface (FSS)-based distributed absorber formed by a series and parallel array consisting of 25 annular antenna elements, each containing two SINIS bolometers. By using a design with 50 bolometers, we reduce incident power load on each bolometer, increase sensitivity and saturation power which is important for ground-based and balloon-borne telescopes with high background power loads. Our main detector pixel is optimized for a frequency band centered at 345 GHz. The detectors are matched to incoming telescope beam by a back-to-back horn with a back reflector. Such a configuration improves both the efficiency and the bandwidth of the receiver. Measured voltage responsivity approaches $2*10^9$ V/W with an amplifier-limited voltage noise of 20 nV/Hz$^{1/2}$, which corresponds to a NEP $= 10^{-17}$ W/Hz$^{1/2}$. The linear voltage response for incoming power is observed for absorbed power of about 5 pW. The current responsivity for parallel array is $2*10^4$ A/W and the shot noise limited intrinsic noise equivalent power is NEP $= 5*10^{-18}$ W/Hz$^{1/2}$. The noise equivalent temperature difference is NETD $= 100$ μK/Hz$^{1/2}$ at 2.7-K background radiation temperature.**

***Index Terms*—Antenna arrays, bolometers, submillimeter wave integrated circuits, superconducting devices.**

I. Introduction

MANY balloon-borne and ground-based high-altitude radio telescopes like BOOMERANG [1], OLIMPO [2], LSPE [3], as well as APEX [4] in Chile, BTA [5] in Russia, and SUFFA [6] in Uzbekistan require both high sensitivity and wide dynamic range to provide measurements with rather high background radiation power load. The superconductor-insulator-normal metal-insulator-superconductor (SINIS) structure is generic for various superconducting devices, namely electron coolers, thermometers, and bolometers. In the pioneering publication [7], NIS junctions were used for temperature sensing of normal-metal absorber. Later theoretically [8] and experimentally [9], it was demonstrated that SINIS structure can provide electron cooling. For SINIS bolometers, one of specific cases is the so-called cold electron bolometer [10] which combines electron cooling and temperature sensing for normal-metal absorber. Some collection of experimental results with single antennas was presented in our earlier publication [11]. Such operation mode with electron cooling has some controversial features for sensitive receivers. Removing of hot electrons by electron cooling is equivalent to increasing the heat sink from absorber, increasing thermal conductivity G, which leads to reducing of absorber temperature and voltage response. Thermal fluctuation noise (aka phonon noise) arises from transferring energy from absorber to the heat sink in quantized portions. For the system in equilibrium $T_{\rm abs} = T_{\rm sink}$, the classical relation is $\mathrm{NEP}^2_{\rm th} = 4\mathrm{kT}^2\mathrm{G}$. In the nonequilibrium electron–phonon system with different electron and phonon temperatures, emission and absorption of phonons are uncorrelated and gives two separate noise terms. Cooling only electrons is not a real advantage for bolometer, because the key parameter is this electron–phonon related $\mathrm{NEP}^2 = 10k\Lambda\Sigma(T_e^6 + T_p^6)$, where T_p is phonon temperature, T_e is electron temperature, Λ is volume of absorber, and Σ is material parameter. Cooling both electrons and phonons can significantly improve NEP. Separate cooling of electrons with heat sinking to superconducting electrodes unavoidably leads to phonon temperature increase in the vicinity of absorber that in turns get rise to NEP increase as T_p^6. The additional negative factor is a shot noise of heat transfer, approximately given by $\mathrm{NEP}^2 = 4kT_0P$, in which P is cooling power, and electron shot noise of dc bias $\mathrm{NEP}^2_{\rm SIN} = 2eI_{\rm dc}/(\mathrm{d}I/\mathrm{d}P)^2$.

Single SINIS bolometer can be saturated already at the power level well below 1 pW. For increasing the dynamic range, we use series and parallel arrays of such bolometers. In this article, we develop our approach in the fabrication of distributed absorber in the form of frequency-selective surface [12]–[14]. Each pair of bolometers is integrated in a planar annular antenna, and as a result, a 25 antenna-SINIS element array can cover a large area. The beam pattern of such an array without phase coherence is very broad. To match to a narrow output beam of telescope, the natural solution is to use a back-to-back horn for each pixel. This design is similar to the one used on the Planck satellite instrument [15] and OLIMPO balloon telescope [2].

Manuscript received May 6, 2019; revised August 19, 2019; accepted August 24, 2019. Date of publication September 16, 2019; date of current version October 3, 2019. The work of A. A. Gunbina was supported by RSCF project 19-32-5002. This article was recommended by Associate Editor C. Kilbourne. *(Corresponding author: Mikhail A. Tarasov.)*

M. A. Tarasov, R. A. Yusupov, A. M. Chekushkin, and D. V. Nagirnaya are with the Kotelnikov Institute of Radio Engineering and Electronics, 125009 Moscow, Russia (e-mail: tarasov@hitech.cplire.ru; yusupovrenat@hitech.cplire.ru; chekushkin@hitech.cplire.ru; darianagirnaya@mail.ru).

A. A. Gunbina and V. F. Vdovin are with the Institute of Applied Physics, 603950 N.Novgorod, Russia (e-mail: aleksandragunbina@mail.ru; vdovin_iap@mail.ru).

S. Mahashabde is with Microtechnology and Nanoscience, Chalmers University of Technology, 41296 Gothenburg, Sweden (e-mail: sumedh.mahashabde@chalmers.se).

V. S. Edelman is with the P. Kapitza Institute for Physical Problems, 117334 Moscow, Russia (e-mail: edelman@kapitza.ras.ru).

G. V. Yakopov is with the Special Astrophysical Observatory, Big Altazimuth Telescope, 369167 Nizhny Arhyz, Russia (e-mail: yakopov@sao.ru).

Color versions of one or more of the figures in this article are available online at http://ieeexplore.ieee.org.

Digital Object Identifier 10.1109/TASC.2019.2941857

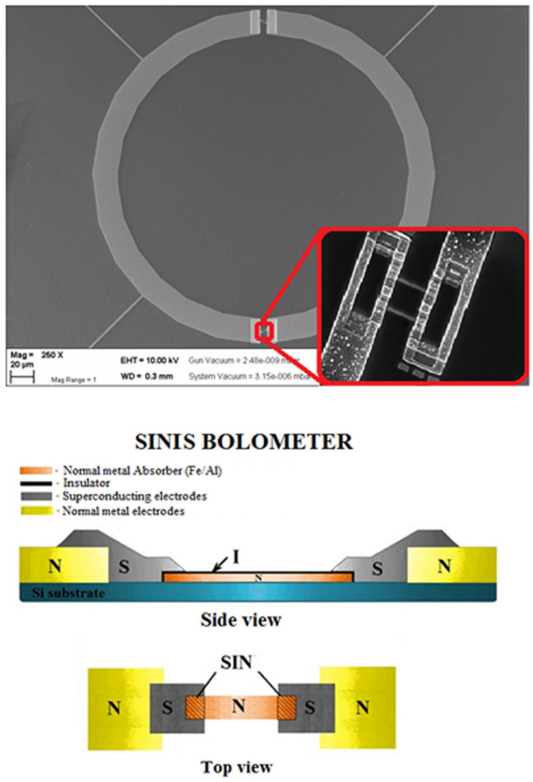

Fig. 1. Single annular antenna and SINIS bolometer (top), schematic of SINIS bolometer (bottom). Two parallel narrow lines in the inset correspond to normal electrode and provide resistance of absorber about 20 Ω.

II. Annular Antenna Array With SINIS Bolometers

We measured two types of annular antenna arrays designed for 350-GHz frequency band. SEM image of antenna and schematic of SINIS bolometer are presented in Fig. 1. Two SINIS bolometers are integrated in a single annular antenna. Choice of annular antenna is advantageous compared to dipole or slot antennas because it provides a lower sidelobes level and lower losses in the substrate modes [12], [13]. Narrow diagonal wires are intended for dc bias and readout. Such elements can be connected in series or in parallel depending on the readout type. We use a bilayer of Fe/Al as the normal metal for the absorber and superconducting Al for the electrodes. The arrays with 25 single antennas were connected in series for the first type of samples, and in parallel for the second type. Such antennas connected in series provide high output resistance that is optimal for current bias and voltage readout. The asymptotic resistance of series array measured at bath temperature of 280 mK is 50 kΩ and maximum dynamic resistance is 4 MΩ. For voltage biased (current readout), we fabricated a parallel array of 25 ring antennas; the normal state resistance for this sample was 14 Ω which is three orders of magnitude less than the case when the detectors are connected in series. For the current bias, the dynamic resistance at optimal bias point with the largest voltage response is about 500 kΩ, and for voltage bias with largest current response, the dynamic resistance is around 10 Ω, so in the first case MOSFET and JFET readout can provide good noise matching, and in the second case SQUID or microwave readout is optimal.

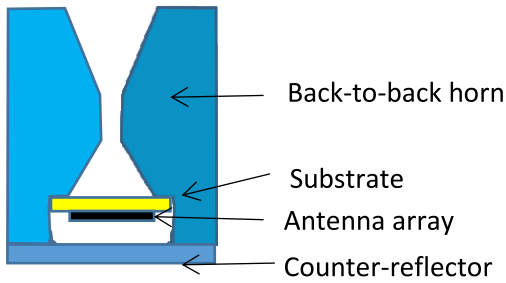

Fig. 2. Schematic view of back-to-back horn with dielectric substrate, antenna array and counter-reflector.

III. Back-to-Back Horn With Dielectric Substrate and Counter-Reflector as Integrating Cavity

For microwave modeling of planar antenna array, it looks attractive to assume a single unit cell that is arranged in the infinite array. Calculations are often limited to *X* and *Y* polarized incident plane waves corresponding to E_x and E_y modes. In CST frequency-domain mode, one can model the system using periodic excitation, which makes the calculation fast, but it does not correspond to more complicated real electrodynamics. In such a simplified modeling, the array of uncorrelated absorbers is substituted by a phased array. As a result, the bandwidth and the beam pattern can be different than the actual performance of this kind of distributed absorber. Here, we consider a model of an integrating cavity that describes more accurately the back-to-back horn with thick substrate and a counter-reflector at some distance from it.

Integrating sphere or cavity is a simple solution for focusing a beam upon the detector. It is a well-developed technique for FIR, mid-IR and NIR bands, and such devices are commercially available from several companies; see, e.g., [16]. Optical design serves well if the integrated detector is homogeneous. When the source is moved, the focused beam will see a different portion of source. The main reasons for using integrating spheres are following: uniform beam pattern for the detector with inhomogeneous beam, isotropic detection even for a detector with preferred directions, reduction of polarization effects from beam and detector, realizing of the whole beampattern of detector including side lobes and back lobes.

Integrating cavity is a highly reflective enclosure placed in close proximity to detector so that the reflected beam enters the cavity, bounces around the highly reflective diffuse surface of walls and finally impinges upon the detector. The main function is spatial integration of the detector beam. The initial beam of detector falling on the cavity surface is scattered in all directions. The detector finally views the integrating sphere with a large solid angle. In order to improve the isotropy of the detection, the sensing element can be placed not in the line of sight for incoming beam. A well-designed sphere will collect all available sidelobes in 2π steradians. The schematic of integrating cavity is presented in Fig. 2. Schematic and photograph of two types of sample holders are presented in Fig. 3.

The integrating cavity throughput is higher because the beam falling on the detector is increased by the multiple reflections of

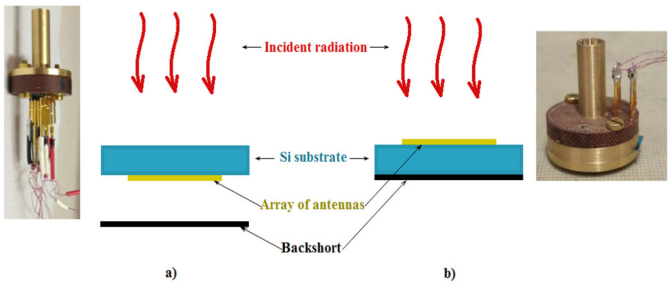

Fig. 3. Schematic picture of sample illumination and photographs of sample holders: (a) from the substrate side and (b) from the antenna side.

the light. The cavity enhances the detected signal by collecting the beam and reflecting it around until it illuminates the detector. The factor of this gain is called the sphere multiplier (M) which is a function of the wall reflectance (ρ_w), and ratio of the area of the input window of sphere to its total area ($f = A_w/A_s$)

$$M = \rho_w/[1 - \rho_w\,(1\ -\ f)]$$

and for $\rho_w = 1$ it is just A_s/A_w. In a practical design, the area of the input window is kept around 5%, wall reflectance is between 95% and 99% and resulting sphere gain is about 10–30.

Integrating spheres can be more efficient than an optical system with an equivalent detector position but have a lower throughput than the direct imaging optics. The reduced throughput can be compensated by the use of the high sensitivity cooled detectors.

Flux density inside the integrating sphere is M times larger than direct illumination. If distributed absorber is perfectly matched to the incoming beam, then power is absorbed even without the integrating cavity. If in some frequency range the detector is more reflective, inside the cavity its multiplier will compensate for such mismatch and finally, after several reflections most of the power will be absorbed even for mismatched loads. As a result, using the integrating cavity makes the spectral response much more uniform and the bandwidth of the incident radiation is now determined by the input quasioptical filter rather than by the detector.

Another important parameter is the factor of losses which is determined not only by the reflectance of surface, but also by losses in on-chip wirings and dc/signal connection lines. The main rule of thumb for integrating spheres is that no more 5% of the sphere surface area is consumed by port openings. In the case of distributed absorber mounted inside back-to-back horn, it makes better matching compared to our measurements of the same samples with immersion sapphire lenses.

IV. Design and Simulation

We studied two illumination configurations: incident beam through the Si substrate [see Fig. 3(a)] [2] and when antenna side of the wafer is facing the incident beam [see Fig. 3(b)]. In the first configuration (a), the substrate thickness was approximately $\lambda^*/2$ and the distance to counter-reflector about $\lambda/4$, in which λ is free-space wavelength, and λ^* is wavelength in dielectric. The resulting bandwidth is about 20 GHz and performance is

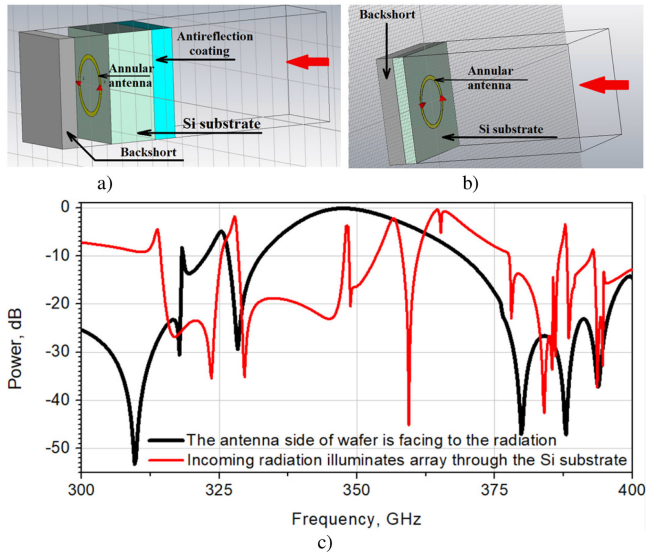

Fig. 4. Unit cells of investigated samples. (a) Standard type, when incoming radiation illuminates array through the Si substrate with antireflection coating. (b) Antenna side of wafer is facing the radiation. (c) Results of modeling.

rather sensitive to the tolerance of both distances. The qualitative description of the drawback of such a configuration is that a half-wavelength dielectric plate is transparent to radiation; signal passes through the substrate, reflects from the backshort, and finally is absorbed by the pixel. In our experiments, we tested several thicknesses of Si substrate: 380, 280, 130, and 65 μm (approximately $3\lambda^*/2$, $2\lambda^*/2$, $\lambda^*/2$, and $\lambda^*/4$, in which λ^* is the wavelength in dielectric), and found out that the half-wavelength case is not the best. According to our measurements, the most efficient configuration [see Fig. 3(b)] is the case when the planar antenna array is facing the radiation, substrate is $\lambda^*/4$ thick and its back side is covered with thick Au film which functions as a backshort. In this case, the position of reflector is exactly 65 μm $= \lambda^*/4$ and together with the back-to-back horn we obtain a very close resemblance to an integrating cavity. As a result, we have improved matching efficiency, spectral bandwidth, and its uniformity.

The CST Studio Suite numerical simulation results for unit cells of investigated samples are shown in Fig. 4. Two SINIS bolometers are integrated in annular antenna. We used discrete ports for the resistance of absorber (40 Ω) and a lumped element for bolometer's capacitance (25 fF). The outer and inner diameters of the ring antenna are 300 and 256 μm. In the presented model, the substrate thicknesses used are 280 μm [see Fig. 4(a)] and 65 μm [see Fig. 4(b)]. The perfect electric conductor boundary was used for backshort modeling in both cases. In experiment, the backshort is made of an aluminum foil or thick gold film. Frequency-domain solver and "unit cell" boundaries were used for simulation. In the case when incident radiation illuminates the array through the Si substrate [see Fig. 4(a)], we use $\lambda^*/4$ antireflection coating for improving sensitivity and uniformity of the spectral response. The simulation results are shown in Fig. 4(c). The absorption efficiency of 50% or more is achieved. Changing the size of array elements

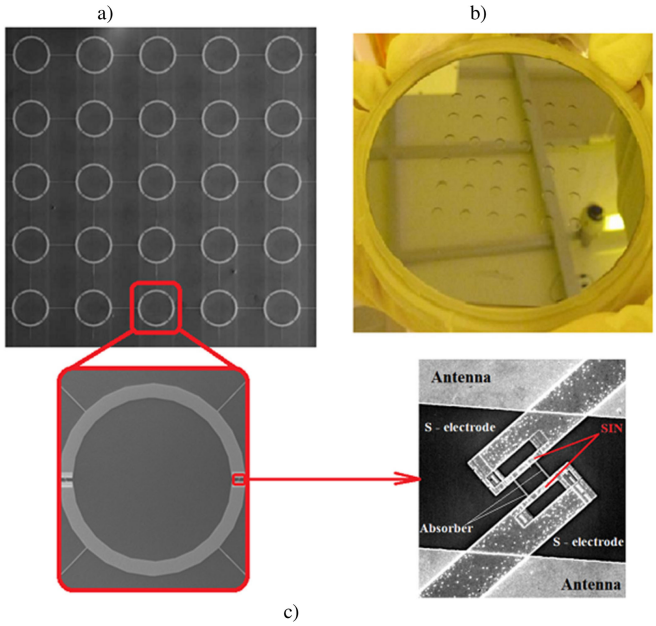

Fig. 5. (a) Array of annular antennas. (b) Back side of wafer with 36 caves each 3 mm in diameter, 250-μm-deep etched in 3 in Si wafer. (c) SEM images of annular antenna and SINIS bolometer.

causes a shift in the resonance frequency. The main conclusion from these simulations is that illumination from the antenna side and counter-reflector from the back side of substrate are advantageous for uniformity and efficiency of spectral response. In practice, we cannot account for all parasitic reflections and losses inside the cavity with substrate and calculate the full system performance with back-to-back horn. The simulation results are used for the first approximation of the investigated structure.

V. Fabrication

Fabrication of antenna array includes just two layers: first layer consisting of antennas, wires, and contact pads, and second with SINIS bolometers. The first layer is patterned by laser lithography and electron-beam deposition of a trilayer metal (10 nm Ti/100 nm Au/20 nm Pd) on the Si substrate. Bolometers are deposited in second layer using shadow evaporation technology. First, the normal metal bilayer of (1.2 nm Fe/14 nm Al) is deposited followed by Al oxidation at a pressure of 10 Torr. This bilayer is nonsuperconducting due to the magnetic proximity effect, and it can be oxidized to form a tunnel barrier. Subsequently, Al superconducting electrode 60+70 nm thick was evaporated at angles $\pm 45°$.

The samples with four different substrate thicknesses were fabricated and investigated. Dry Silicon plasma etching was used to achieve necessary substrate thicknesses of 65 and 127 μm. The substrates are thinned on the side opposite to the antenna array. For the other samples, with substrate thicknesses of 280 and 380 μm, we used 2 and 3 in substrates of standard thicknesses. In case when the antenna side of wafer is facing the radiation, the opposite side is covered by thick gold layer which functions as a backshort. The fabricated samples are shown in Fig. 5.

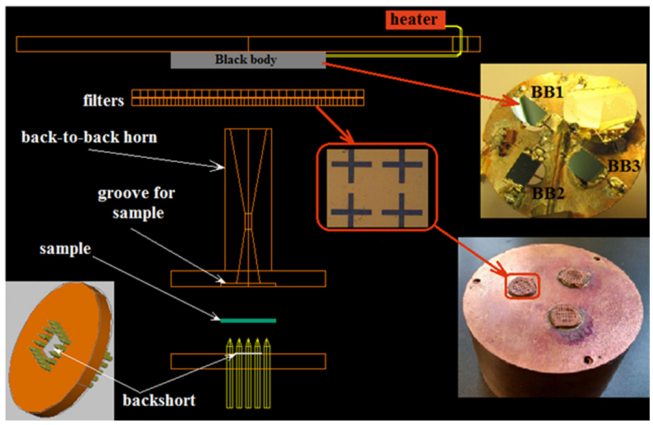

Fig. 6. Schematics of optical response measurements with cold blackbody source inside cryostat and photograph of such setup inside cryostat. One can see three blackbody sources (BB1, BB2, BB3) and three band-pass filters at the bottom right panel.

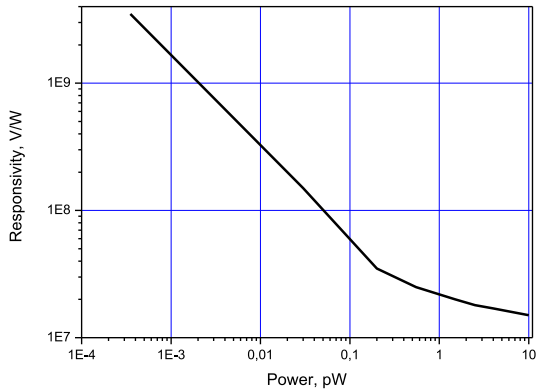

Fig. 7. Responsivity dependence on power for single bolometer in the series array measured at 100 mK with cryogenic blackbody source.

VI. Optical and Spectral Response Measurements

Quasistatic optical response to incoming radiation was measured in a dilution cryostat [17] using cold blackbody radiation source made of NiCr film on silicon or sapphire substrates. The radiation source was equipped with a thermometer; it was heated by dc current and mounted on the 2.7 K stage. Schematic of optical response measurements, blackbody, and filter photograph is shown in Fig. 6. Between such source and back-to-back horn with the sample, we placed a double band-pass filter at the same temperature as sample holder. The results of such optical responsivity measurements are shown in Fig. 7. In an additional experiment, the blackbody source was outside the cryostat switching between hot and cold load at temperatures 300 and 77 K.

For spectral response measurements, we use a 230–380 GHz backward wave oscillator (BWO) illuminating the input aperture of a back-to-back horn via the cryostat's optical window and three neutral density filters (NDFs) with transmission below –10 dB placed at radiation shields 100, 3, and 0.3 K temperature stages. NDF were fabricated from a NiCr film with a sheet resistance of 350 Ω/square on a thin KAPTON film. Two channels

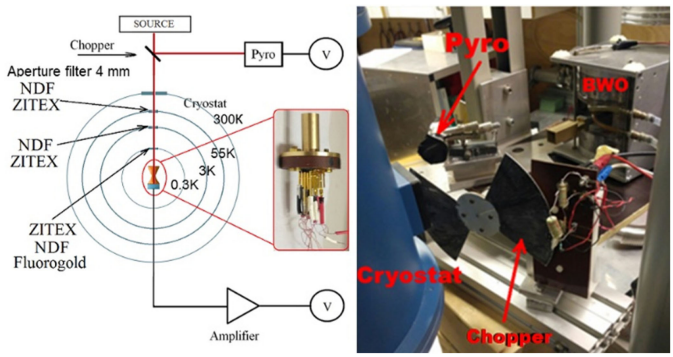

Fig. 8. Schematics and photograph of the spectral measurements with BWO source, chopper as a beam switch, and a pyroelectric detector in reference channel. NDF is a home-made NDF with –10 dB transmission; ZITEX and Fluorogold are commercial IR filters.

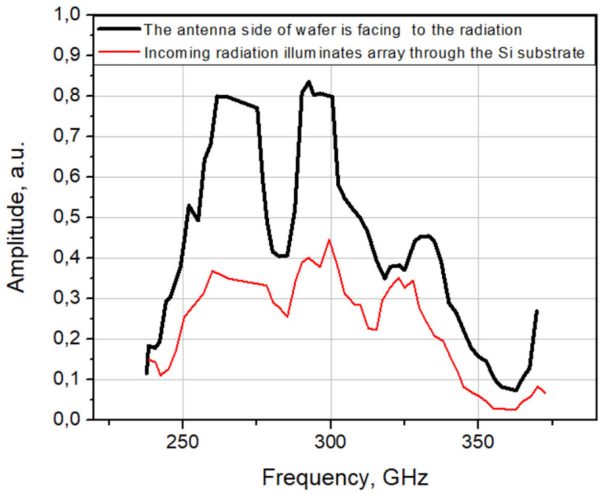

Fig. 9. Spectral response for sample illuminated from the antenna side and from the substrate side.

were measured simultaneously by a lock-in amplifier, one for signal from the bolometer, and another from a pyroelectric detector which monitored the level of the incoming power. Schematic image and photograph of the spectral response measurements are presented in Fig. 8. For comparing the level of the received signal in both samples (illuminating from substrate and when antenna side of wafer is facing to the radiation), the experiment was performed in one measurement cycle. The spectral response is presented in Fig. 9.

VII. Discussion

For a practical background power load level, the equivalent electron temperature of bolometers in our experiments is higher than 230 mK even when the phonon temperature is below 100 mK. In the case of strong overheating of the absorber, the dynamics is different from that expected for the equilibrium case. In this case, we do not see strong variations of responsivity d*V*/d*P* on the incoming signal power and observe dynamic range over 30 dB. In the case when there is no strong overheating both by background power and by signal power itself, the variations of absorber temperature can be described with high accuracy by electron–phonon interaction by standard relation $P_{\rm sig} = \sum \nu (T_e^5 - T_0^5)$, where $\sum = 3 \cdot 10^9$ W $\cdot$ m^{-3} $\cdot$ K^{-5} is a material parameter similar to the AlMn alloy [18], ν is absorber volume, T_e is electron temperature, and T_0 is phonon temperature. In this case, the electron–phonon thermal conductivity $G_{\rm ep} = dP/dT_e = 5 \sum \nu T_e^4$, this corresponds to voltage responsivity

$$S = \frac{dV}{dP} = \frac{dV}{dT} \cdot \frac{dT}{dP} = \frac{dV}{dT} \frac{1}{G} = \frac{dV}{dT} \cdot \frac{1}{5 \sum \nu T^4}. \quad (1)$$

If we assume the maximum for temperature response from [19] for aluminum NIS junctions as $dV/dT = V_\Delta / T_e T_e =$ 4 mV/K for ideal case and $dV/dT = 20$ k/e $= 2$ mV/K for practical cases, then for a single SINIS bolometer with absorber volume of $\nu = 2 \cdot 10^{-20}$ m^3, the responsivity is $S = 5 \cdot 10^6 / T^4$. This corresponds to $1.2 \cdot 10^{10}$ V/W for an electron temperature 0.1 K. For an array comprising of 50 such bolometers, the absorber volume is 50 times as much and responsivity estimation drops down to 2.4 10^8 V/W. Even if we avoid overheating by stray background power, still, the absorption of a high signal will bring significant increase in the electron temperature which will directly affect the responsivity according to [19]

$$S_\nu^{\max} = \frac{4k}{e} \frac{1}{(\sum \nu)^{0.2}} \frac{1}{P^{0.8}}. \quad (2)$$

The important feature of this formula is that it does not contain phonon temperature of bolometer; actually, it depends on electron temperature which is determined by absorbed power of the signal. For the current responsivity, the dependence on electron temperature is even clearer; in the first approximation [19], it is $S_i = e/(2kT_e)$.

Now, we can compare responsivity for a single bolometer and a series array of bolometers illuminated by a single-mode horn for the same blackbody radiation temperature. Initial parameters are the following: absorber volume for single bolometer $\nu = 0.02$ μm^3, background radiation power $P_1 = 1$ pW for a single mode which corresponds to $T_{bb} = 5$ K in our bandwidth of 20 GHz. The observed overheating of absorber is $T_e = 0.43$ K. For one bolometer, the responsivity should be $S_1 = 2{*}10^8$ V/W and the output voltage response $V_{\rm out1} = S_1 P_1 = 200$ μV. As an example, if the power load is reduced by factor of 10 down to 0.1 pW, this leads to single bolometer responsivity increase up to $2.6{*}10^9$ V/W due to the gain factor of $G = (P_1/P_2)^{0.8} = 6.3$. In our single annular antenna, we have two bolometers, absorbed signal power in each is 0.5 pW, overheating to $T_e = 0.38$ K (not $T_e = 0.43$ K), voltage responsivity of two bolometers in parallel is approximately *the same* as for one bolometer $S = 1.3{*}10^8$ V/W, *not* twice as low as one can suppose due to twice as low power absorbed in bolometer.

For the array with $n = 50$ bolometers in the integrating cavity with the same single-mode input waveguide, the signal power for one bolometer is $P_{1/50} = P/50$ times as low compared to full power P, but antennas are connected in series and output signal is $G_{\rm ser} = 25$ times as much (two bolometers in parallel in each ring). For one bolometer in the array, the responsivity $S_{1/50} = S_1 G_{50}$ will be $G_{50} = (50)^{0.8} = 23$ times as high compared to the full power load responsivity of single bolometer S_1, but

the signal power is 50 times as low, and sum signal on the series array

$$V_{\text{out}} = (S_1 * G_{50})\,(P/n)\,G_{\text{ser}} = (S_1 P) * 11. \tag{3}$$

As a result, in the high *signal power limited* case, we can get 11 times as much voltage response of series array compared to the single bolometer for the same signal power. In the *background limited case*, the higher dynamic range can be achieved, but with the price of lower responsivity and higher NEP. All practical cases are background limited; the background power is >1 pW while the signal power is three orders of magnitude lower. Until the signal power is below the background level, the responsivity is unchanged and the dynamic range *D* is determined by ratio of this background power to the NEP at this power load

$$D = \frac{P_{bg}}{\text{NEP}} = \frac{P_{bg} * S_v}{V_n} = \frac{2k}{e * V_n}\left(\frac{P_{bg}}{\Sigma\nu}\right)^{0.2}. \tag{4}$$

In our case for $P_{bg} = 1$ pW, $V_n = 20\ \text{nV}/\text{Hz}^{1/2}$, and $\nu = 2{*}10^{-20}$ m^3 for a single bolometer, we get $D = 3.8{*}10^3$ or 35 dB. For the array of 50 bolometers, *D* slowly decreases as volume $\nu^{0.2} \sim (50)^{0.2} = 2.2$. As soon as signal level exceeds the level of background power load, the responsivity decreases as $P^{0.8}$ and the output signal decreases too. In our case, this happens already at blackbody temperature over 5 K and further increase of blackbody temperature to 10 K leads to heating power increase up to 5 pW and three times decline of responsivity.

VIII. Conclusion

For improving the dynamic range and sensitivity of SINIS bolometers, we fabricated array consisting of 25 annular antennas each containing two SINIS bolometers optimized for a frequency band centered at 345 GHz. Doing so, we reduced the incident power load on each bolometer, and increased the sensitivity and saturation power, which are important for ground-based and balloon-borne telescopes with high background power loads. The detectors are matched to incoming telescope beam by three and five-mode back-to-back horns with a back reflector. We have measured the arrays at temperatures down to 80 mK. Optical responsivity was measured in the 350 GHz band with a variable temperature cold blackbody radiation source and bandpass filters. Spectral bandwidth in the 240–380 GHz range was measured using a BWO source. The measured voltage responsivity approaches $2 * 10^9$ V/W with an amplifier-limited voltage noise of 20 $\text{nV}/\text{Hz}^{1/2}$, which corresponds to NEP = 10^{-17} $\text{W}/\text{Hz}^{1/2}$. The linear voltage response for incoming power is observed for absorbed power of about 5 pW. The current responsivity for parallel array is $2{*}10^4$ A/W and the shot noise limited intrinsic noise equivalent power is NEP = $5{*}10^{-18}$ $\text{W}/\text{Hz}^{1/2}$. The noise equivalent temperature difference is NETD = 100 $\mu\text{K}/\text{Hz}^{1/2}$ at 2.7-K background radiation temperature level, and is suitable for measurements of anisotropy of cosmic microwave background radiation.

Acknowledgment

This work was carried out at the IREE RAS within the framework of the state task. The fabrication was carried out using USU 352529 facilities.

References

[1] S. Masi *et al.*, "Instrument, method, brightness, and polarization maps from the 2003 flight of BOOMERanG," *Astron. Astrophys.*, vol. 458, pp. 687–716, 2006, doi: 10.1051/0004-6361:20053891.

[2] S. Masi, "Images of mm/sub-mm sky with stratospheric balloon experiments," *Adv. Space Res.*, vol. 34, no. 3, pp. 483–490, 2004, doi: 10.1016/j.asr.2003.04.032.

[3] P. de Bernardis *et al.*, "SWIPE: A bolometric polarimeter for the large-scale polarization explorer," *Proc. SPIE*, vol. 84523, 2012, Art. no. 8452F, doi: 10.1117/12.926569.

[4] R. Gusten, L. A. Nyman, P. Schilke, K. Menten, C. Cesarsky, and R. Booth, "The Atacama Pathfinder EXperiment (APEX)—A new submillimeter facility for southern skies," *Astron. Astrophys.*, vol. 454, no. 2, pp. L13–L16, 2006, doi: 10.1051/0004-6361:20065420.

[5] 2012. [Online]. Available: https://www.sao.ru/Doc-en/Telescopes/bta/descrip.html

[6] A. Hojaev, G. Shanin, and Y. Artyomenko, "Suffa radio observatory in Uzbekistan: Progress and radio-seeing research plans," *Proc. Int. Astron. Union*, vol. 2, no. SPS5, pp. 177–182, 2006, doi: 10.1017/S1743921307006965.

[7] M. Nahum, P. Richards, and C. Mears, "Design analysis of a novel hot-electron microbolometer," *IEEE Trans. Appl. Supercond.*, vol. 3, no. 1, pp. 2124–2127, Mar. 1993, doi: 10.1109/77.233921.

[8] M. Nahum, T. Eiles, and J. Martinis, "Electronic microrefrigerator based on a normal-insulator-superconductor tunnel junction," *Appl. Phys. Lett.*, vol. 65, 1994, Art. no. 3123, doi: 10.1063/1.112456.

[9] M. Leivo, J. Pekola, and D. Averin, "Efficient Peltier refrigeration by a pair of normal metal/insulator/superconductor junctions," *Appl. Phys. Lett.*, vol. 68, 1996, Art. no. 1996, doi: 10.1063/1.115651.

[10] L. Kuzmin, I. Devyatov, and D. Golubev, "Cold-electron bolometer with electronic microrefrigeration and general noise analysis," *Proc. SPIE*, vol. 3465, pp. 193–199, 1998, doi: 10.1117/12.331165.

[11] M. Tarasov, L. Kuzmin, V. Edelman, S. Mahashabde, and P. de Bernardis, "Optical response of a cold-electron bolometer array integrated with a 345 GHz cross-slot antenna," *IEEE Trans. Appl. Supercond.*, vol. 21, no. 6, pp. 3635–3639, Dec. 2011, doi: 10.1109/TASC.2011.2169793.

[12] S. Mahashabde *et al.*, "A frequency selective surface based focal plane receiver for OLIMPO balloon-borne telescope," *IEEE Trans. THz Sci. Technol.*, vol. 5, no. 1, pp. 145–152, Jan. 2015, doi: 10.1109/TTHZ.2014.2362010.

[13] S. Mahashabde, A. Sobolev, M. Tarasov, G. Tsydynzhapov, and L. Kuzmin, "Planar frequency selective bolometric array at 350 GHz," *IEEE Trans. THz Sci. Technol.*, vol. 5, no. 1, pp. 37–43, Jan. 2015, doi: 10.1109/TTHZ.2014.2377247.

[14] S. Mahashabde *et al.*, "A distributed-absorber cold-electron bolometer single pixel at 95 GHz," *Appl. Phys. Lett.*, vol. 107, 2015, Art. no. 092602, doi: 10.1063/1.4929604.

[15] J.-M. Lamarre *et al.*, "Planck prelaunch status: The HFI instrument, from specification to actual performance," *Astron. Astrophys.*, vol. 520, pp. 1–20, 2010, doi: 10.1051/0004-6361/200912975.

[16] Integrating Spheres, PIKE Technologies, 2019. [Online]. Available: www.piketech.com

[17] V. S. Edelman, "A dilution microcryostat-insert," *Instrum. Exp. Techn.*, vol. 52, no. N2, pp. 301–307, 2009, doi: 10.1134/S002044120902033X.

[18] G. C. O'Neil, P. J. Lowell, J. M. Underwood, and J. N. Ullom, "Measurement and modeling of a large-area normal-metal/insulator/superconductor refrigerator with improved cooling," *Phys. Rev. B*, vol. 85, 2012, Art. no. 134504, doi: 10.1103/PhysRevB.85.134504.

[19] D. Golubev and L. Kuzmin, "Nonequilibrium theory of a hot-electron bolometer with normal metal-insulator-superconductor tunnel junction," *J. Appl. Phys.*, vol. 89, 2001, Art. no. 6464, doi: 10.1063/1.1351002